Charge-dependent electronic stopping of swift nonrelativistic heavy ions

Peter Sigmund
Physics Department, Odense University, DK-5230 Odense M, Denmark
(Received 3 June 1997)

The stopping of swift nonrelativistic heavy ions has been analyzed theoretically as a function of the projectile charge q_1. Excitation and ionization of target electrons are described within Bohr's classical theory and the limitations toward Bethe's quantal description are outlined. For oxygen ions in carbon the Bethe regime is found to be confined to the velocity range where the ion is essentially stripped in charge equilibrium. The effect of projectile electrons is taken into account mainly via screening of the Coulomb interaction, but excitation of projectile electrons is discussed briefly. The significance of projectile screening hinges on a parameter s that depends on projectile and target parameters and varies substantially over the electron shells of the target. Calculated fixed-charge stopping cross sections agree well with measured values in absolute magnitude and in their variation with charge state. q_1^2 scaling frequently has been assumed in the literature. A continuous transition is predicted between such scaling and a stopping power that is almost independent of the projectile charge. [S1050-2947(97)05411-5]

PACS number(s): 34.50.Bw, 61.85.+p, 52.40.Mj, 79.20.Rf

I. INTRODUCTION

The stopping of ions penetrating through matter is governed by a number of scattering processes such as (i) excitation and ionization of target electrons, (ii) electron capture, (iii) projectile excitation and ionization, and (iv) recoiling nuclei. While this classification is not unique and individual processes are not necessarily uncoupled, existing theory [1–5] has, by and large, been based on this scheme or slight modifications thereof with considerable success. The relative significance of these processes depends primarily on the speed v and the atomic number Z_1 of the penetrating ion and to some extent on target parameters and projectile state. In the following, ''swift'' refers to ions with $v > v_0 = e^2/\hbar$, the Bohr velocity, and ''heavy'' refers to $Z_1 \gg 1$.

For swift ions nuclear stopping (iv) is small and only weakly coupled to electronic stopping (i)–(iii) [1,6]. This process will not be considered in the present study. Electronic stopping is best understood for swift light ions since target excitation and/or ionization dominates and Coulomb forces are weak enough to encourage the use of perturbation theory [1,2,7,8]. For heavier ions the validity of perturbation theory becomes questionable and the role of projectile electrons needs attention [1].

A. Bloch theory

The electronic stopping power $-dE/dx$ is commonly written in the form

$$-\frac{dE}{dx} = NS = \frac{4\pi Z_1^2 e^4}{mv^2} N Z_2 L, \tag{1}$$

where S is the stopping cross section, N and Z_2 are the density and atomic number of target atoms, m and $-e$ are the electron mass and charge, and L is the stopping number. For a bare ion the standard expression is Bloch's formula [9]

$$L_{\mathrm{Bloch}} = L_{\mathrm{Bethe}} + \Delta L = \ln \frac{2mv^2}{I} + \mathrm{Re}\left[\psi(1) - \psi\left(1 + i\frac{Z_1 v_0}{v} \right) \right], \tag{2}$$

where I denotes the mean excitation energy of a target atom, ψ the digamma function [10], and Re the real part. Equation (2) needs shell and polarization (Barkas) corrections at low velocities and density and relativistic corrections at high velocities [2,8]. Moreover, Eq. (2) ignores electron capture. The physical basis underlying Bloch's formula has been confirmed and extended recently [11]. For light ions the Bloch correction ΔL in Eq. (2) becomes small and L_{Bloch} reduces to the Bethe formula [7],

$$L_{\mathrm{Bethe}} = \ln \frac{2mv^2}{I}, \tag{3}$$

which follows from first-order quantal perturbation theory.

Figure 1 shows L_{Bloch} as a function of the scaled velocity variable $v/Z_1 v_0$. A universal plot, valid for all Z_1 and Z_2, has been generated by subtraction of a constant term $\ln(2mv_0^2 Z_1^2/I)$. Disregard for a moment the fact that L_{Bloch} drops below zero below a certain threshold velocity. It is seen that L_{Bloch} is made up of two distinct logarithmic

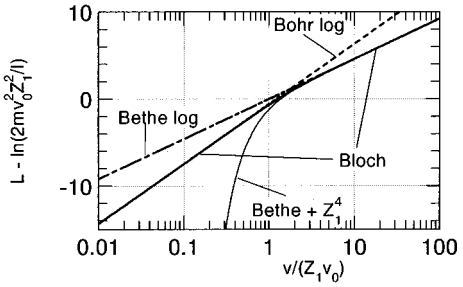

FIG. 1. Comparison of the Bloch stopping number L for a bare ion with limiting expressions on a universal plot. Solid line, L_{Bloch}; dashed lines, L_{Bethe} and L_{Bohr}; thin line, L_{Bethe} amended by Z_1^4 correction.

branches intersecting at $v=2.25Z_1v_0$. Above this point $L_{\rm Bloch}$ rapidly approaches the Bethe logarithm (3). The logarithmic curve below the intersection reflects the classical Bohr formula [12]

$$L_{\rm Bohr}=\ln\frac{Cmv^3}{Z_1e^2\omega},\quad C=1.1229, \tag{4}$$

where ω stands for a characteristic resonant frequency of the target. In the present context one may identify ω with $I/\hbar$.

The velocity interval of interest, $v_0<v<c$ is equivalent to a range $Z_1^{-1}<v/Z_1v_0<137/Z_1$ for the scaled variable in Fig. 1. For light ions this interval lies almost completely in the right half of the graph, i.e., the Bethe regime. Conversely, for very heavy ions it falls predominantly into the Bohr regime. For intermediate ions such as for $Z_1\sim10$, there is a Bethe regime at high and a Bohr regime at low velocities. The physical origin of this distinction has been discussed in detail [1].

Note that interpolation between the two logarithmic expressions is necessary only over a very narrow velocity range around the intersection. In that region, ΔL may be approximated by its high-speed expansion [8]

$$\Delta L\sim-1.202\left(\frac{Z_1v_0}{v}\right)^2. \tag{5}$$

The resulting expression for L also has been included in Fig. 1 (Bethe$+Z_1^4$). It is clear that this expansion is valid only when ΔL is small, but would yield unreasonable results when applied at low values of v/Z_1v_0. Considering the Bloch correction ΔL as *synonymous* with Eq. (5), i.e., a Z_1^4 correction to the stopping power, is appropriate only for very light ions.

The implications of Fig. 1 have not entered existing tabulations of heavy-ion stopping powers [5,13–16], which are all based on quantal perturbation theory. Figure 1 shows that this, taken as an isolated feature, will overestimate stopping powers. When a Bloch correction was applied, only the Z_1^4 term was included [17]. Figure 1 shows that this tends to underestimate stopping powers.

$L_{\rm Bloch}$ drops below zero below some threshold velocity dependent on Z_1 and Z_2. The same is true for the Bethe logarithm, although the threshold is lower and therefore less disturbing. The appearance of negative stopping cross sections is not a consequence of the underlying physical model but of the use of asymptotic (high velocity) expansions in the evaluation. For the Bethe theory this artifact has been eliminated long ago [2,18]. For the Bohr and the Bloch theory this was done recently [19].

B. Effective charge

Swift heavy ions carry typically a number of electrons. With increasing penetration depth the ionic charge q_1e fluctuates around a certain equilibrium value, which is commonly estimated from an expression of the type of [20,21]

$$q_{\rm eq}e\simeq Z_1e(1-e^{-v/v_{\rm TF}}), \tag{6}$$

where $v_{\rm TF}=Z_1^{2/3}v_0$ is the Thomas-Fermi velocity. The resulting screening of the Coulomb field of the nuclear charge must affect the stopping power. As a first estimate it is common to replace the nuclear charge Z_1e by an effective charge [20] $q_{\rm eff}e$, which in general depends on the impact parameter.

Attempts have been made to establish a theoretical basis for the effective charge [22–25], all starting from quantal perturbation theory and therefore limited to light ions, even though this is not commonly recognized. One of the models [22] has in fact been applied to generate stopping-power tables that include high-Z_1 ions [5].

Frequently, the effective charge has been treated as an empirical parameter to be determined from Northcliffe's scaling rule [3]

$$-\frac{dE}{dx}=(q^2)_{\rm eff}\left(-\frac{dE}{dx}\right)_{Z_1=1}, \tag{7}$$

where $(-dE/dx)_{Z_1=1}$ is the stopping power for a bare proton. However, the stopping power is not generally proportional to a power of the charge and, unlike for protons, heavy-ion stopping powers are not governed by the Bethe theory.

The second problem can be overcome by an alternative definition, going over the stopping fraction or fractional effective charge

$$\mathcal{F}=\frac{(-dE/dx)_{q_1}}{(-dE/dx)_{\rm bare}}, \tag{8}$$

where q_1 is the ion charge and $(-dE/dx)_{\rm bare}$ the stopping power for the bare ion (charge Z_1e). This ensures that the two quantities that are compared belong into comparable regimes of stopping theory. A valid calculation of this quantity allows predictions on the dependence of the stopping power on the ion charge q_1.

The former problem is essentially unsolved: It is by no means obvious that the effective charge number $q_{\rm eff}$ replacing Z_1 in Eq. (1) should be identical to or just similar to the one to be replaced in Eq. (2), as has been implied in Ref. [17]. The Bloch correction ΔL originates in close collisions; hence the effective charge entering there ought to be rather close to the nuclear charge.

C. Processes involving projectile electrons

The role of projectile electrons is not restricted to statically screening the Coulomb force of the projectile nucleus. Charge exchange affects the stopping process both through the dependence of the stopping cross section on q_1 and through the energy lost in charge transfers [1]. Another source of energy loss is projectile excitation by scattering on target electrons and/or nuclei. Standard theory of projectile excitation and ionization follows closely that of target processes [1], while electron capture belongs into an altogether different category.

Quite independent of the processes taken into account, the statistics of stopping no longer obeys Eq. (1) when changes in projectile state occur and the stopping cross section depends on the state. Instead of a single stopping cross section, statistics is then governed by a stopping matrix $\|S_{IJ}\|$, where I and J label the projectile state before and after an individual collision [26–28]. Elements S_{IJ} of the stopping matrix

have been extracted from measurements of heavy-ion energy losses differential in entrance and exit state versus foil thickness [29]. If the equilibrium population comprises n significant projectile states, a reliable estimate of the stopping power may require up to n^2 stopping cross sections S_{IJ}.

D. Scope of present work

This work represents a followup on a recent study of the stopping of bare ions [19] that extended the range of practical applicability of the Bohr and Bloch theory down to velocities where Fig. 1 predicts major inadequacies of the Bethe formula. The modified Bohr formula resulting from that work was found to reproduce the qualitative behavior of the stopping power for the O-Si system surprisingly well even without allowance for necessary low-velocity corrections. This encouraged an extension of the theory to ions carrying electrons. The primary goal of the present study has been to explore the role of projectile screening in the velocity range where the Bloch theory reduces to the Bohr limit. When combined with a parallel treatment on the basis of the Born approximation, this treatment provides charge-dependent stopping cross sections over a wide range of velocities and projectiles. Allowance for projectile excitation extends the range of applicability of the theory even further. However, estimates of the contribution of electron capture to nondiagonal elements of the stopping matrix will not be presented here because such estimates cannot be obtained from the Bohr theory or a related classical model. Therefore, pertinent data for comparison with experiment are fixed-charge stopping cross sections rather than equilibrium stopping powers.

II. QUALITATIVE CONSIDERATIONS

A. Screening and adiabatic radius

Consider a projectile ion screened by $N_1=Z_1-q_1$ electrons distributed over a screening radius a. The range of effective interaction between a swift *point charge* interacting with a bound target electron is confined by Bohr's adiabatic radius [12]

$$a_{\mathrm{ad}}=\frac{v}{\omega}, \tag{9}$$

where ω is a (classical) resonant frequency of a target electron. A qualitative measure of the importance of projectile screening is found by considering the ratio a_{ad}/a: For $a_{\mathrm{ad}}/a\ll 1$ the projectile-target interaction will essentially be that of a point charge, while screening becomes significant for $a_{\mathrm{ad}}/a\gtrsim 1$.

B. Bohr limit

For a point charge, Bohr's theory [12,19] predicts a stopping number $L(\xi)$ dependent on the variable

$$\xi=\frac{mv^3}{Z_1e^2\omega}, \tag{10}$$

which reduces to Eq. (4) at high speed ($\xi\gg 1$). Expressing the velocity dependence in a_{ad} by the Bohr parameter ξ, one finds

$$\frac{a_{\mathrm{ad}}}{a}=\frac{1}{a}\left(\frac{Z_1e^2\xi}{m\omega^2}\right)^{1/3}. \tag{11}$$

Now, assume Thomas-Fermi scaling where

$$a=a_{\mathrm{TF}}g\left(\frac{q_1}{Z_1}\right),\quad a_{\mathrm{TF}}=\frac{0.8853\,a_0}{Z_1^{1/3}}, \tag{12}$$

a_0 being the Bohr radius and $g(q_1/Z_1)$ a dimensionless function of the charge fraction so that $g(0)=1$ for a neutral projectile. With this, Eq. (11) reads

$$\frac{a_{\mathrm{ad}}}{a}=\frac{s\xi^{1/3}}{0.8853\,g(q_1/Z_1)}, \tag{13}$$

where

$$s=\left(\frac{Z_1e^2/a_0}{\hbar\omega}\right)^{2/3}. \tag{14}$$

The velocity-independent parameter s is a measure of the importance of screening at given ξ and projectile charge fraction.

If the target is characterized by a single resonant frequency $\omega=I/\hbar$, and if Bloch's relation [30]

$$I\simeq Z_2I_0 \tag{15}$$

with [18] $I_0\simeq 10$ eV is inserted for the mean excitation energy, then Eq. (14) reduces to

$$s\simeq 2\left(\frac{Z_1}{Z_2}\right)^{2/3}. \tag{16}$$

It is seen that at constant ξ and q_1/Z_1 the significance of screening increases with increasing Z_1 and decreasing Z_2 and that s is equally sensitive to the target as to the projectile. This finding is in contrast to the rather common assumption of an effective-charge parameter independent of the material [13].

A more detailed analysis would start at the spectrum of resonant frequencies. Then the increase in s with decreasing ω reflects the longer range of interactions with outer electrons, which are therefore more sensitive to projectile screening.

C. Bethe limit

In the Bethe limit the stopping number L depends on the Bethe parameter

$$\xi'=\frac{2mv^2}{\hbar\omega}, \tag{17}$$

in accordance with Eq. (3). Then Eq. (13) changes into

$$\frac{a_{\mathrm{ad}}}{a}=\frac{s'\xi'^{1/2}}{0.8853g(q_1/Z_1)}, \tag{18}$$

with

$$s'=\left(\frac{Z_1^{2/3}e^2/2a_0}{\hbar\omega}\right)^{1/2} \tag{19}$$

or, with the Bloch relation (15), $s' \simeq 1.2 Z_1^{1/3}/Z_2^{1/2}$. This leads to the same qualitative conclusions as in the Bohr limit.

III. BOHR THEORY

A. Close and distant collisions

In the Bohr theory [12] interactions between a bare projectile and target electrons are classified into close and distant collisions according to impact parameters below or above a certain critical value p_0. Close interactions are assumed to obey the law of free Coulomb scattering, while distant interactions are governed by a time-dependent field induced by the projectile at the *rest position* of the target electron. The electron is bound to this position by a harmonic-oscillator force with a resonant frequency ω.

Bohr's treatment will be generalized here to an ion carrying electrons. This generalization is straightforward in the case of distant collisions, while the opposite limit leaves a couple of options, the feasibility of which needs discussion.

B. Dipole limit

The contribution from distant interactions to the energy loss T in an individual scattering event is evaluated from the expression

$$T = \frac{1}{2m} \left| \int_{-\infty}^{\infty} dt \mathbf{F}(t) e^{-i\omega t} \right|^2, \tag{20}$$

where $\mathbf{F}(t) = -\boldsymbol{\nabla} V$ is the force acting on a harmonically bound target electron in its equilibrium position. Consider an ion in uniform motion along a trajectory $\mathbf{R(t)} = \mathbf{p} + \mathbf{v}t$ and accompanied by N_1 electrons in parallel trajectories $\mathbf{R}_\nu(t) = \mathbf{R}(t) + \mathbf{r}_\nu$, $\nu = 1,\ldots,N_1$, with $\mathbf{p}$ denoting the vectorial impact parameter from the target electron to the ion trajectory. Then Eq. (20) reduces to

$$T = \frac{2\pi^2 e^2}{m} \int d^3k \int d^3k' (\mathbf{k}\cdot\mathbf{k}') V^*(\mathbf{k}) V(\mathbf{k}') e^{i(\mathbf{k}-\mathbf{k}')\cdot\mathbf{p}} \times \delta(\omega + \mathbf{k}\cdot\mathbf{v})\, \delta(\omega + \mathbf{k}'\cdot\mathbf{v}), \tag{21}$$

where $V(\mathbf{k})$ is the Fourier transform of the potential,

$$V(\mathbf{k}) = \frac{e}{2\pi^2 k^2} F(\mathbf{k}), \quad F(\mathbf{k}) = Z_1 - \sum_{\nu=1}^{N_1} e^{-i\mathbf{k}\cdot\mathbf{r}_\nu}, \tag{22}$$

V^* the complex conjugate, and $\delta(\,)$ the Dirac function. Equation (21) can be rewritten in the form

$$T = \frac{e^4}{2\pi^2 m v^2} \left(\left| \frac{\omega}{v} B(\mathbf{p}) \right|^2 + \left| \boldsymbol{\nabla}_{\mathbf{p}} B(\mathbf{p}) \right|^2 \right), \tag{23}$$

where

$$B(\mathbf{p}) = \int \frac{d^2 k_\perp}{k_\perp^2 + (\omega/v)^2} F\left(\mathbf{k}_\perp, -\frac{\omega}{v} \right) e^{-i\mathbf{k}_\perp\cdot\mathbf{p}} \tag{24}$$

and $\mathbf{k}_\perp$ is the component of $\mathbf{k}$ in the direction of $\mathbf{p}$.

Alternatively one may average Eq. (21) over the distribution of (independent) projectile electrons via

$$\overline{F^*(\mathbf{k}) F(\mathbf{k}')} = [Z_1 - N_1 \phi(k)][Z_1 - N_1 \phi(k')] + N_1 [\phi(|\mathbf{k}-\mathbf{k}'|) - \phi(k)\phi(k')], \tag{25}$$

where

$$\phi(k) = \overline{\left(\frac{\sin k r_\nu}{k r_\nu} \right)}. \tag{26}$$

This yields

$$T = T_1 + T_2, \tag{27}$$

where T_1 is the leading contribution for $Z_1 \gg 1$,

$$T_1 = \frac{2e^4}{m v^2} \left\{ \left| \frac{\omega}{v} A\left(\frac{\omega p}{v} \right) \right|^2 + \left| \frac{\partial}{\partial p} A\left(\frac{\omega p}{v} \right) \right|^2 \right\}, \tag{28}$$

with

$$A\left(\frac{\omega p}{v} \right) = \int_0^\infty \frac{k_\perp dk_\perp}{k_\perp^2 + \omega^2/v^2} J_0(k_\perp p) \times \left[Z_1 - N_1 \phi\left(\sqrt{k_\perp^2 + \frac{\omega^2}{v^2}} \right) \right], \tag{29}$$

while T_2 contains terms proportional to N_1 in Eq. (25) that become insignificant for $Z_1 \gg 1$. J_0 is a Bessel function in standard notation [10].

The integral over $k_\perp$ can be carried out for a charge distribution characteristic of exponential screening,

$$\frac{1}{4\pi r a^2} e^{-r/a}, \tag{30}$$

so that

$$T(p) \simeq T_1 = \frac{2 Z_1^2 e^4}{m v^2} \left(\frac{\omega}{v} \right)^2 f(p), \tag{31}$$

with

$$f(p) = [\beta K_1(\zeta) + \delta\alpha K_1(\alpha\zeta)]^2 + [\beta K_0(\zeta) + \delta K_0(\alpha\zeta)]^2 \tag{32}$$

and

$$\beta = \frac{q_1}{Z_1}, \quad \delta = \frac{N_1}{Z_1}, \quad \zeta = \frac{\omega p}{v}, \quad \alpha = \sqrt{1 + \left(\frac{a_{\mathrm{ad}}}{a} \right)^2}. \tag{33}$$

The K_ν are modified Bessel functions in standard notation [10]. Bohr's result [12] is recovered in the limits of $\beta = 1$ and/or $a = \infty$.

An alternative and more direct derivation of Eq. (32) could be obtained by replacing the Coulomb interaction in Bohr's original calculation by a screened potential equivalent to the charge distribution (30). This possibility was recognized some time ago for the special case of a neutral projectile [31]. However, the present calculation shows that there is a correction term T_2 that can be neglected only for $Z_1 \gg 1$, and it illuminates the relation to form factors appearing in the Bethe theory.

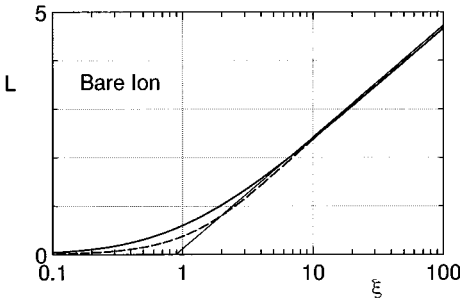

FIG. 2. Stopping number for a point charge evaluated from classical theory. $\xi = mv^3/Z_1 e^2 \omega$. Thin line, Bohr logarithm [12]; solid line, from Ref. [19]; dashed line, Eq. (36).

C. Wide-angle extrapolation: Point charge

Consider first the case of a point charge ($\beta = 1$). At small impact parameters the energy loss (31) reduces to

$$T(p) \sim \frac{2Z_1^2 e^4}{mv^2 p^2}, \tag{34}$$

which becomes infinite at $p = 0$. However, the replacement

$$p^2 \to p^2 + p_0^2, \tag{35}$$

with $p_0 = Z_1 e^2/mv^2$, turns Eq. (34) into Rutherford's law, which is appropriate for close collisions. One may tentatively make the substitution (35) for *all* impact parameters. This has little effect at large p, but allows integration of the stopping cross section $S = \int T(p) 2\pi\, p\, dp$ in closed form, with the result

$$L = \xi^{-1} K_0(\xi^{-1}) K_1(\xi^{-1}), \tag{36}$$

which is readily seen to reduce to Bohr's original formula (4) at large ξ.

Equation (36) represents a modification of Bohr's stopping formula that extends the meaningful behavior down to lower projectile speeds than the original version (4), which turns negative near $\xi = 1$. An alternative extrapolation was found recently [19]. Figure 2 shows a comparison between the two results as well as the Bohr logarithm. It is seen that the difference between the two extrapolations is noticeable for $\xi = mv^3/Z_1 e^2 \omega \lesssim 5$ and significant for $\xi \lesssim 2$. While the error margin in L for $\xi \lesssim 2$ appears larger than one might like it to be, other effects, especially polarization corrections which are neglected presently, may cause errors of similar magnitude.

D. Wide-angle extrapolation: Dressed ion

Within the spirit of the Bohr theory, close collisions are to be treated as free collisions between the projectile and the target electron. For a structured projectile two limiting cases offer themselves for consideration. If the spacing between projectile particles exceeds the collision diameter of Coulomb scattering one may view close collisions as an incoherent superposition of individual Rutherford events. Conversely, for closely spaced projectiles the dressed ion can be viewed as a stiff charge distribution so that the dynamics is governed by screened Coulomb scattering. Before establishing criteria to distinguish between the two extremes, let us look at the respective predictions.

1. Incoherent scattering

For independent Coulomb scattering of the projectile and its electrons on a target electron, the energy transfer reads

$$T = \frac{2Z_1^2 e^4}{mv^2(p^2 + p_0^2)} + \sum_\nu \frac{2e^4}{mv^2[(\mathbf{p} + \mathbf{p}_\nu)^2 + p_0'^2]}, \tag{37}$$

where p_0 was introduced in Eq. (35), $p_0' = 2e^2/mv^2$, and $\mathbf{p}_\nu$ is the component of the electron coordinate $\mathbf{r}_\nu$ in the direction of $\mathbf{p}$. It is implied that only one of the terms on the right-hand side is significant in any individual interaction.

The maximum value of any of the electron terms in Eq. (37) amounts to 1/4 of the ionic term. Therefore, an estimate is necessary to establish whether or not the electonic terms, which must be roughly proportional to N_1, can be ignored after integration over the impact parameter. In the average over all orientations the maximum influence must be expected at $\mathbf{p} = \mathbf{0}$. Here the right-hand side of Eq. (37) reduces to

$$\frac{2Z_1^2 e^4}{mv^2 p_0^2}\left[1 + N_1 \left(\frac{p_0}{Z_1 a}\right)^2 G\left(\frac{p_0'}{a}\right)\right], \tag{38}$$

where $G(\eta) = \int_0^\infty dt\; t \exp(\eta \sinh t)$ for the charge distribution (30). The physical picture can be valid only for $p_0, p_0' \ll a$, i.e., it implies that $\eta = p_0'/a$ is small. Numerical evaluation shows that $G(\eta) \sim 4\eta^{-1/4}$ in that limit. Hence the relative significance of the sum of the electronic terms in Eq. (38) is

$$\sim \frac{4N_1}{Z_1^2}\left(\frac{p_0}{a}\right)^2 \left(\frac{a}{p_0'}\right)^{1/4}. \tag{39}$$

This expression is dominated by the first two factors and therefore is clearly $\ll 1$. Thus a collision at impact parameter $p = 0$ is a Rutherford collision between the unscreened ion and a target electron.

The above estimate assumed classical scattering between electrons accompanying the projectile and target electrons. While this assumption is not justified, the fact that this contribution to the stopping power is negligible for $Z_1 \gg 1$ renders this difference immaterial.

Now, in the same limit Eq. (32) reduces to $f(p) = 1/\zeta^2$. This can be joined to Rutherford's law by the substitution (35) in Eq. (32). The remaining integral can be carried out and the final expression for the stopping number reads

$$\begin{aligned} L = \zeta_0 [\beta^2 K_0(\zeta_0) K_1(\zeta_0) + \delta^2 \alpha K_0(\alpha\zeta_0) K_1(\alpha\zeta_0) \\ + 2\beta\delta K_1(\zeta_0) K_0(\alpha\zeta_0)] - \frac{\delta^2}{2}(\alpha^2 - 1)\zeta_0^2 \{[K_1(\alpha\zeta_0)]^2 \\ - [K_0(\alpha\zeta_0)]^2\}, \end{aligned} \tag{40}$$

where $\zeta_0=\omega p_0/v$. Apart from standard recursion relations for Bessel functions, integration formulas have been employed, which are listed in Ref. [10].[1]

2. Coherent scattering

For coherent interaction the appropriate wide-angle extrapolation is the binary scattering law applying to a screened ion, taken as a stiff charge distribution and hitting a target electron. For a repulsive interaction a substitution of the type of Eq. (35) has been applied successfully in the description of *elastic* ion-atom scattering [6] with the difference that the parameter p_0 was chosen such as to satisfy conservation laws in the limit of $p=0$. The validity of the procedure is less obvious for attractive interaction since the scattering angle in the center-of-mass system may exceed 180° in this case, with the consequence of oscillatory effects at small impact parameter. Disregarding this potential source of error, let us apply a substitution

$$p^2\rightarrow p^2+p_0''^2, \tag{41}$$

with p_0'' fixed by conservation laws, i.e., $T(p=0)=2mv^2$, the maximum permissible energy transfer in a free binary collision between a heavy particle and a target electron at rest. In dimensionless variables this reduces to

$$f(\zeta_0'')=\xi^2, \tag{42}$$

where $\zeta_0''=\omega p_0''/v$. Integration then yields a stopping number given by Eq. (40) with ζ_0 replaced by ζ_0''. $L=L(\xi)$ can then be tabulated from Eqs. (42) and (40), ζ_0'' being taken as the independent variable [19].

3. Coherent versus incoherent scattering

If the target atom is considered as an entity, i.e., if no differentiation is made between the electron shells, the transition from predominantly coherent to predominantly incoherent scattering takes place when the ratio p_0/a drops below ~ 1. In dimensionless units this is equivalent to

$$\xi>\left(\frac{s}{0.8853g(\beta)}\right)^{3/2}. \tag{43}$$

While incoherent scattering thus tends to prevail at high and coherent scattering at low ξ, the limiting value varies proportionally to Z_1/Z_2 according to Eqs. (43) and (16). For $Z_1\gg Z_2$ that limit is reached only at quite high values of ξ. Conversely, for $Z_1\ll Z_2$, incoherent scattering will dominate over most of the pertinent velocity range. This is consistent with experience from light-ion stopping [32,33].

E. Screening radius

For numerical estimates information is needed about $g(\beta)$, Eq. (12) describing the dependence of the ionic screening radius on charge state. Screening functions may be determined from Thomas-Fermi theory [34]. In that description, positive ions have a finite radius r_0. Potentials are written in the form

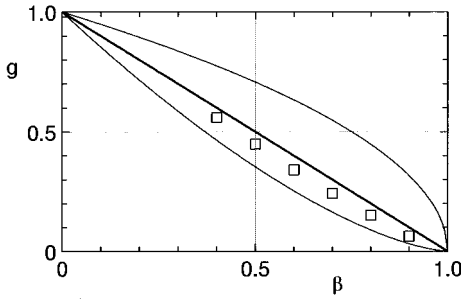

FIG. 3. Ratio $a/a_{\mathrm{TF}}=g$ versus charge fraction β extracted from Thomas-Fermi theory by matching to the exponentially screened Coulomb potential (squares). Lines represent Eq. (45) with $r=0.5,1.0,1.5$ (top to bottom).

$$V(r)=\begin{cases}\dfrac{Z_1e}{r}\phi_{\mathrm{TF}}\left(\dfrac{r}{a_{\mathrm{TF}}}\right)+\dfrac{q_1e}{r_0} & \text{for} \quad r<r_0\\[2ex] \dfrac{q_1e}{r} & \text{for} \quad r>r_0,\end{cases} \tag{44}$$

where ϕ_{TF} can be estimated by a procedure of Fermi and Amaldi [35,36]. $g(\beta)$ has been determined by matching the potential equivalent to the charge distribution (30) to Eq. (44). The result is shown Fig. 3. Within the accuracy of an exponential fit to a Thomas-Fermi screening function, it appears justified to adopt the expression

$$g(\beta)=(1-\beta)^r=\delta^r. \tag{45}$$

With the exception of Fig. 5, explicit evaluations reported below assume $r=1$.

F. Evaluation

The stopping number $L(\xi)$ has been tabulated for both incoherent and coherent scattering. Since α depends on v and hence on ξ, iteration was necessary in the coherent case starting from a trial value of α. Three iterations have been adequate in all cases. Results are shown in Fig. 4 for four values of s [Eq. (14)]. Figure 5 shows results for $s=10$ evaluated with different values of r [Eq. (45)] characterizing the dependence of the screening radius on the charge state. While an influence is noticeable, it appears weaker than the effect of the absolute value of the screening radius, which acts as an inverse variation in s; cf. Eq. (13).

Figure 4 shows that higher stopping numbers are obtained for coherent than for incoherent scattering. This stems from the fact that the limiting impact parameter p_0 for unscreened Coulomb scattering is too large in the presence of screening. In agreement with the considerations made in Sec. III D 3, the relative difference increases with increasing s and decreasing ξ. Moreover, the relative difference is largest for low charge fracions $\beta=q_1/Z_1$. However, the relative difference is significant mainly for $\xi\lesssim 5$ and it nowhere exceeds the difference between the two predictions of the stopping number for a bare ion in Fig. 2. While the range $\xi\leqslant 5$ is of considerable interest in applications, we need to keep in

[1]Caution had to be exerted with regard to signs (specifically Eqs. 11.3.29 and 11.3.31).

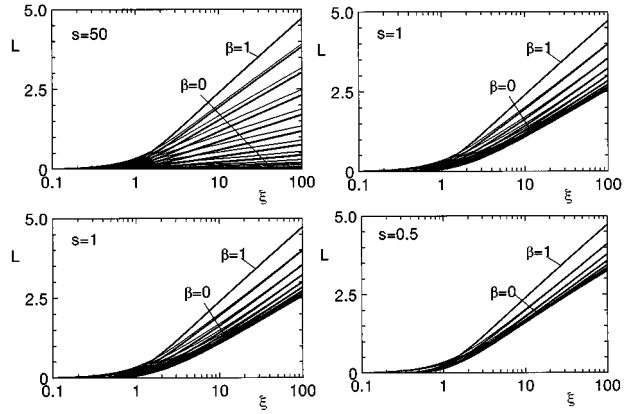

FIG. 4. Stopping number versus the Bohr parameter $\xi = mv^3/Z_1 e^2 \omega$ for the fractional charge $\beta = q_1/Z_1$ varying from 0 to 1 in steps of 0.1. Thick lines, close collisions treated as incoherent Coulomb scattering; thin lines, close collisions treated as screened Coulomb (coherent) scattering. The four graphs refer to different values of s [Eq. (14)].

mind that this is also the regime where a substantial Barkas correction must be expected, although reliable estimates for heavy ions are not available, as discussed below. Moreover, estimates on the basis of coherent scattering suffer from uncertainties regarding scattering angles exceeding 180°, mentioned in Sec. III D 1. Consequently, despite a systematic underestimate of stopping cross sections on the basis of incoherent scattering for large s, small ξ, and low β, several numerical results reported below have been based upon this model for definiteness as well as analytical and numerical convenience.

It is seen from Fig. 4 that the stopping number is very sensitive to the ionic charge for $s = 50$ and 10, while for $s = 1$ and 0.5 a much weaker dependence is found. Stopping fractions have been plotted in Fig. 6. The central role of the scaling parameter s together with the charge state β is evident, while the variation with ξ is much less pronounced, in particular for large s, where $\mathcal{F}$ is essentially independent of ξ. Figure 7 shows values of the stopping fraction $\mathcal{F}$ at $\xi = mv^3/Z_1 e^2 \omega = 100$ versus the ionic charge fraction $\beta = q_1/Z_1$. The result for $s = 50$ coincides very closely with a q_1^2 dependence, which has often been implied and occasionally been found in experiments [37]. Here this emerges only in the limit of high-Z_1 ions.

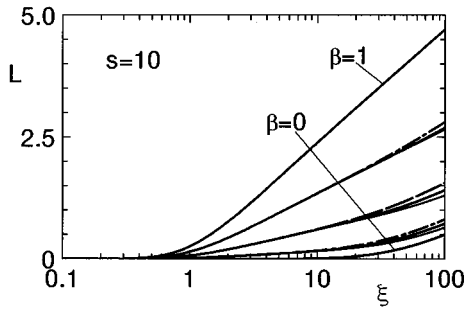

FIG. 5. Illustration of the influence of the parameter r in Eq. (45) on the stopping number L for $s = 10$. The five groups of curves refer to $\beta = q_1/Z_1$ running from 1 to 0 in steps of 0.25 (top to bottom). The fine structure corresponds to $r = 1.5$ (thin solid lines), 1.0 (thick solid lines), and 0.5 (dashed lines).

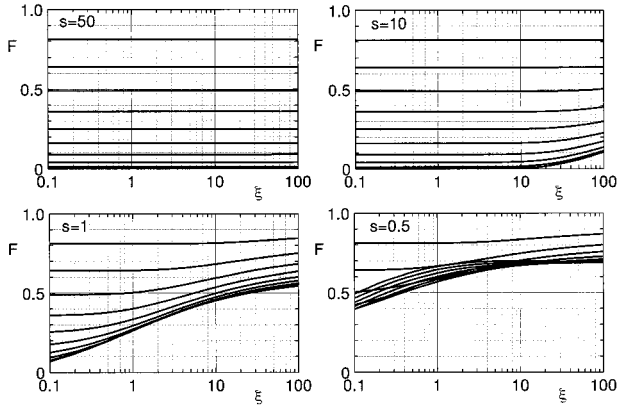

FIG. 6. Stopping fractions $\mathcal{F}$ defined in Eq. (8). Otherwise the notation is as in Fig. 4. Only incoherent scattering is shown.

G. Projectile excitation

A full treatment of projectile excitation or ionization is outside the scope of the present paper since this is at least as much a problem of statistics as of atomistics. However, a few comments are appropriate.

For a given projectile state the contribution of projectile excitation to the total inelastic energy loss may be found by symmetrization, i.e., adding a term in which the roles of projectile and target are interchanged. Denoting the cross section for target excitation evaluated above by S_{12}, we have to add a term of the form

$$S_{21} = \frac{4\pi Z_2^2 e^4}{mv^2} N_1 \mathcal{F}(s_{21}, \beta_2, \xi_{21}) L_0(\xi_{21}), \tag{46}$$

where $\mathcal{F}$ is the stopping fraction introduced in Eq. (8),

$$\xi_{21} = \frac{mv^3}{Z_2 e^2 \omega_1 h(\beta_1)}, \quad s_{21} = \left(\frac{Z_2 e^2/a_0}{\hbar \omega_1 h(\beta_1)} \right)^{2/3}. \tag{47}$$

Here $\hbar\omega_1$ is the mean excitation energy of a neutral projectile and $h(\beta_1)$ accounts for the variation of this quantity with charge state. L_0 is the modified Bohr stopping number for a bare nucleus.

For a neutral target we obtain the expression for the ratio between the stopping cross sections for projectile and target excitation,

$$\frac{S_{21}}{S_{12}} = \frac{Z_2}{Z_1} \frac{N_1}{Z_1} \frac{\mathcal{F}(s_{21}, 0, \xi_{21})}{\mathcal{F}(s_{12}, \beta_1, \xi_{12})} \frac{L_0(\xi_{21})}{L_0(\xi_{12})}, \tag{48}$$

where quantities characterizing target excitation have been labeled similarly and $h(\beta_2) = 1$. Now, Bloch's relation (15) indicates that $Z_2 \omega_1 \simeq Z_1 \omega_2$. Hence the variation of the ratio of L_0 functions is governed by the logarithm of $h(\beta_1)$ and thus weak. For a neutral projectile Eq. (48) reduces to

$$\frac{S_{21}}{S_{12}} \simeq \frac{Z_2}{Z_1} \frac{\mathcal{F}(s_{21}, 0)}{\mathcal{F}(s_{12}, 0)}, \tag{49}$$

where the weak dependence of $\mathcal{F}$ on ξ has likewise been ignored. The two factors vary in opposite directions and at comparable rates. Hence, for a neutral projectile and not too widely different Z_1 and Z_2, projectile and target excitation and ionization yield comparable contributions to the stopping

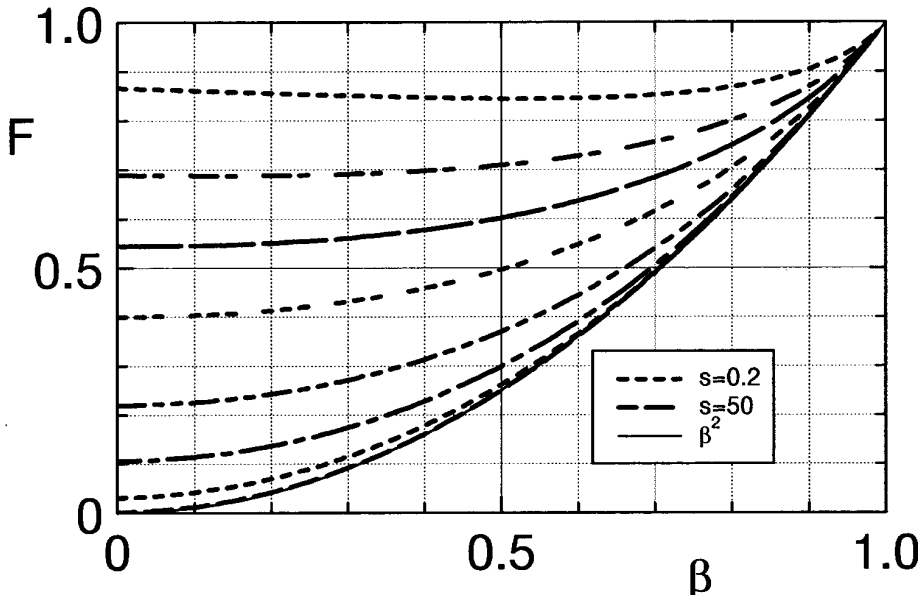

FIG. 7. Values of the stopping fraction $\mathcal{F}$ at $\xi=100$ plotted as a function of the ionic charge fraction $\beta=q_1/Z_1$. Dashed curves, $s=0.2,0.5,1,2,5,10,20,50$ (top to bottom); thin solid line, $\mathcal{F}=\beta^2$.

cross section. With increasing projectile charge both N_1/Z_1 and the ratio of stopping ratios $\mathcal{F}$ in Eq. (48) decrease, with the consequence of dominating target excitation.

For the purpose of estimating fixed-charge stopping cross sections, the above procedure overestimates the contribution due to projectile electrons since only projectile excitation contributes, while projectile ionization enters nondiagonal elements of the stopping matrix. For neutral projectiles with $Z_1 \gg 1$ this is a major reduction. For highly charged projectiles one may assume hydrogenlike behavior, i.e., excitation and ionization should contribute about equally. On the other hand, for highly charged ions projectile excitation and/or ionization is of minor importance altogether, as indicated above.

In summary, the relative contribution to the stopping cross section from projectile excitation and/or ionization decreases with increasing projectile charge. Its contribution to equilibrium stopping powers is substantial for neutral projectiles while a minor perturbance to fixed-charge stopping cross sections.

IV. BETHE THEORY

When Bethe's theory of stopping [7] is carried out for a dressed ion a form factor enters [23,24,38] so that the contribution from target processes to the stopping number may be written in the form

$$L=\frac{1}{2}\sum_j f_j \int_{Q_{\min}}^{2mv^2} \frac{dQ}{Q}\, G(Q), \tag{50}$$

where the f_j are dipole oscillator strengths characterizing the energy levels ϵ_j of the target, normalized according to $\Sigma_j f_j=1$, and $Q_{\min}=(\hbar\omega_j)^2/2mv^2$ with $\hbar\omega_j=\epsilon_j-\epsilon_0$. The form factor

$$G(Q)=\sum_{l} \left| \left(1-\frac{1}{N_1}\sum_{\nu=1}^{N_1} e^{i\mathbf{q}\cdot\mathbf{r}_\nu} \right)_{l0} \right|^2, \quad Q=\frac{\hbar^2 q^2}{2m} \tag{51}$$

involves the projectile states labeled by l and can be evaluated in straight analogy to the classical case. For independent electrons one finds

$$G(Q)\simeq[1-\delta\phi(k)]^2, \tag{52}$$

where $\phi(k)$ and δ are the quantities introduced in Eqs. (26) and (33), respectively, and terms proportional to N_1/Z_1^2 have been ignored just as in the classical case. For exponential screening (30) one finds

$$G(Q)=\left(\frac{Q+\beta Q_1}{Q+Q_1}\right)^2, \quad Q_1=\frac{\hbar^2}{2ma^2}. \tag{53}$$

Equation (50) excludes shell corrections. For heavy ions the Bethe limit is reached at higher projectile speeds than for

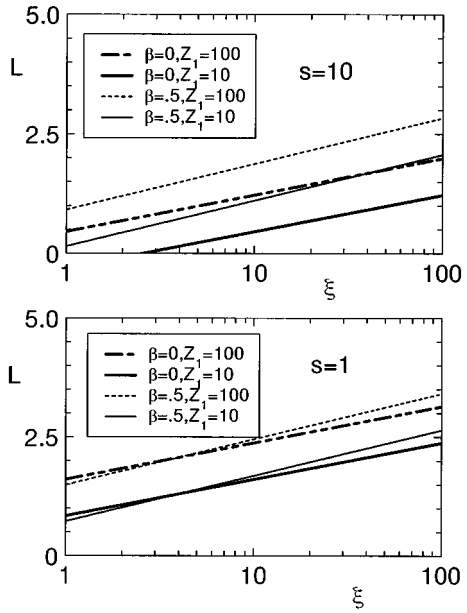

FIG. 8. Bethe stopping number plotted in variables appropriate to Bohr scaling. Upper graph, $s=10$; lower graph, $s=1$.

TABLE I. Parameters governing the comparison with experiments in Tables II and III. $\kappa=2Z_1v_0/v$ separates the Bohr from the Bethe regime [1]. Values for ω_j and f_j tabulated in Ref. [45] were employed because of convenience and easy access, even though subshells are not weighted in accordance with the straight oscillator strengths in Refs. [43, 44] from which they originate.

Ion target	Energy (MeV/u)	κ		$1s$	$2s$	$2p$
C-C[a]	3	1.091	s	0.508	3.272	3.927
			ξ	13.37	218.9	287.8
O-C[a]	3	1.455	s	0.615	3.964	4.757
			ξ	10.03	164.2	215.8
^{58}Ni-C[b]	1.034	8.672	s	1.417	9.138	10.97
			ξ	0.580	9.49	12.48

[a]Reference [41].
[b]Reference [42].

light ions. Hence the neglect of shell corrections is justified for $Z_1 \gg 1$ (cf. also Sec. VI B). Since the leading shell corrections are proportional to v^{-2} and v^{-4} [2], terms of this type will be neglected. With this one finds

$$L=\beta^2 \ln\frac{2mv^2}{I}+(1-\beta^2)\ln\frac{2mav}{\hbar}-\frac{1}{2}(1-\beta)^2, \quad (54)$$

with $\ln I=\Sigma_j f_j \ln(\hbar\omega_j)$. This reduces to $L_{\rm Bethe}$ for a point charge ($\beta=1$) and to

$$L=\ln\frac{2mav}{\hbar}-\frac{1}{2} \quad (55)$$

in the opposite extreme of a neutral projectile. As in the classical case, the contribution from projectile excitation or ionization to the stopping cross section may be obtained by interchanging the roles of target and projectile. This is rigorous within the first Born approximation [23,38].

Standard stopping theory for an electron gas [39] has been applied to screened projectiles [22,25]. It is shown in the Appendix that this theory also leads to Eq. (54).

Equation (55) predicts a stopping cross section for target processes dependent on Z_2, the number of electrons per atom, but no other target parameters. This originates in the fact that for a neutral projectile the limiting impact parameter for target excitation is given by the screening radius of the projectile instead of the adiabatic radius through which binding frequencies enter. It is easily verified that Eq. (55) reflects free Coulomb collisions between the projectile nucleus and the target electrons with a cutoff energy transfer $T_{\rm min}=2.718Q_1$.

Equation (54) is easily seen to depend on the parameter s' only through an additive term $-\ln s'$. Going over to stopping fractions would remove this basic simplicity and therefore discourages one from using stopping fractions in this limit.

In the present context Eq. (54) is of interest mainly for the identification of the upper limit of validity of the modified Bohr theory. Therefore, it is useful to write it down in terms of the variables ξ and s. This yields

$$L=\frac{1}{3}(1+\beta^2)\ln\xi+\left(\beta^2-\frac{1}{2}\right)\ln s+\ln(2Z_1^{1/3}) +(1-\beta^2)\ln[0.8853g(\beta)]-\frac{1}{2}\delta^2. \quad (56)$$

An explicit dependence on Z_1 remains in this expression. A few examples shown in Fig. 8 indicate a greater sensitivity to Z_1 than to the fractional charge $\beta=q_1/Z_1$. The fact that L increases significantly with increasing Z_1 at constant ξ and β confirms that the transition from Bohr-like to Bethe-like behavior moves up rapidly to greater values of ξ with increasing Z_1 at all values of β.

V. APPLICATIONS

A. Fixed-charge stopping cross sections

Cowern *et al.* [29,40,41] measured charge-selected energy-loss spectra with 3 MeV/u carbon and oxygen ions penetrating amorphous carbon foils. Fixed-charge stopping cross sections were extracted by careful analysis based on the Winterbon formalism [26]. Data for $\simeq$1 MeV/u ^{58}Ni ions on carbon were reported recently [42].

The present estimate was done on the basis of bundled oscillator strengths [43–45]. Pertinent parameters are shown in Table I. It is seen that the C and O data lie near the transition between the Bohr and the Bethe regime, as ex-

TABLE II. Calculated and measured [41] stopping cross sections S (keV Å^2/atom) for carbon and oxygen ions in carbon, with target excitation or ionization only and incoherent scattering assumed.

Ion target	Charge state	$L_{\rm Bohr}$	$L_{\rm Bloch}$	$S_{\rm theor}$	$S_{\rm expt}$
C-C	6+	4.688	4.370	0.753	0.714±0.003
	5+	3.478	3.160	0.544	0.519±0.004
O-C	8+	4.398	3.927	1.202	1.108±0.018
	7+	3.439	2.968	0.908	0.933±0.018
	6+	2.790	2.319	0.710	0.735±0.22

TABLE III. Calculated and measured [42] stopping powers $-dE/dx$ [keV/(μg/cm^2)] of carbon for nickel, with target excitation or ionization only. Calculations are given for both coherent and incoherent scattering, with the latter in parentheses.

Ion target	Charge state	L_{Bohr}	L_{Bloch}	$(-dE/dx)_{\mathrm{theor}}$	$(-dE/dx)_{\mathrm{expt}}$
^{58}Ni-C	18+	0.853(0.702)	0.849(0.698)	46.0(37.8)	52.7
	16+	0.706(0.555)	0.702(0.551)	38.0(29.8)	47.5
	13+	0.501(0.369)	0.497(0.365)	26.9(19.74)	40.2
	8+	0.271(0.148)	0.267(0.143)	14.5(7.75)	22.5

pressed by Bohr's kappa parameter $\kappa=2Z_1v_0/v$, while the Ni data lie clearly in the classical regime. Hence there is a noticeable difference between L_{Bohr} and L_{Bloch} in the former case. It is also seen that the data cover a wide range of values of both s and ξ. Note the pronounced variations from shell to shell.

Table II shows a comparison of calculated with measured stopping cross sections for carbon and oxygen ions [41]. Discrepancies range from 3% to 8% in either direction. Apart from potential experimental errors and errors in the data analysis, which could have been underestimated by the authors, the main source of discrepancy is likely to lie in the treatment of target K electrons, which contribute $\sim$20% of the total stopping number. In particular, at $\xi\sim10$ there must be a noticeable Barkas correction (see below). Since the ions are almost stripped, projectile excitation must be a minor perturbation, while improved input on atomic oscillator strengths is likely to produce noticeable changes.

For Ni bombardment Table III shows larger discrepancies. In view of the small values of ξ (cf. Table I), stopping cross sections were evaluated both for coherent and incoherent scattering. The difference is seen to be substantial and, as expected, better agreement is achieved for coherent scattering, although stopping cross sections are underestimated in both cases. Now, unlike the data from Ref. [41], which are the result of a detailed analysis, Ref. [42] did not separate the energy loss suffered under charge exchange. Moreover, projectile excitation is not negligible and increases with decreasing charge state. The discrepancy in Table III shows a similar trend. There must also be a (positive) Barkas correction, but that is more likely to show the opposite tendency.

Fixed-charge stopping cross sections have been measured long ago for light ions at keV [46,47] and more recently at MeV energies [48]. More directly related to the present work are measurements with swift heavy ions under channeling conditions [37,49]. In this geometry interactions with core electrons are suppressed and the leading resonance governing s becomes the plasma frequency ω_P of the conduction electrons. Since $\hbar\omega_P\sim e^2/a_0$ one finds $s\simeq Z_1^{2/3}$, according to Eq. (14). Figure 7 shows that the stopping fraction in that case comes close to being proportional to q_1^2. This is in agreement with the main finding in those experiments. Further support is drawn from the fact that minor deviations from q_1^2 scaling were found for the lowest charge states [49] corresponding to $\beta=0.6$ for sulphur and chlorine ions. Deviations from q_1^2 scaling were positive, in agreement with Fig. 7.

Similar conclusions emerge from more recent experiments on energy losses of channeled Br and Kr ions [50] at 10–15 MeV/u, i.e., $\kappa\simeq3$. The fixed-charge energy loss of highly stripped ions was found to scale well proportionally to q_1^2, in complete agreement with Fig. 7 for $s\simeq10$.

B. Oxygen on carbon

Figure 9 shows fixed-charge stopping powers of carbon for oxygen ions as a function of the ion energy for fully stripped and neutral ions, respectively. The graphs differ not only in absolute magnitude, but also in the position of the

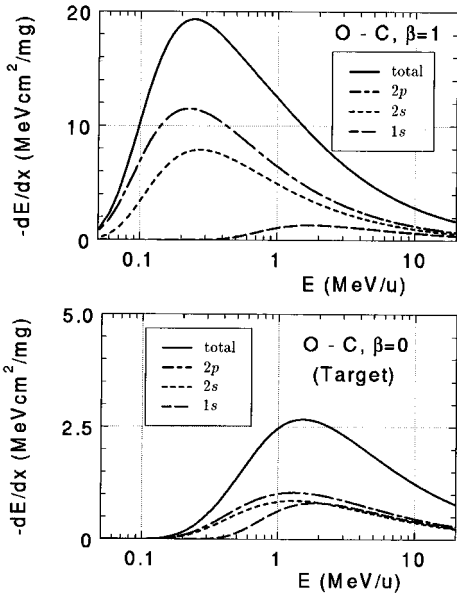

FIG. 9. Calculated stopping power of carbon for oxygen ions. Contribution from target excitation or ionization separated into contributions from three target shells (f_j and ω_j tabulated in [45]). Modified Bohr theory and incoherent scattering are shown. Upper graph, bare ion; lower graph, neutral ion.

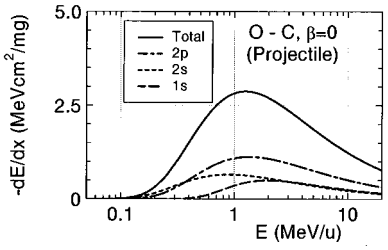

FIG. 10. Calculated stopping power of carbon for neutral oxygen ions from projectile excitation or ionization, separated into contributions from three projectile shells (f_j and ω_j tabulated in [45]). Modified Bohr theory and incoherent scattering are shown.

stopping maximum and the relative contributions from the three subshells: Screening affects mainly $2s$ and $2p$ excitations. For qualitative orientation the contribution from projectile excitations has been evaluated for neutral oxygen (Fig. 10). A behavior very similar to that of target excitation is found, except for a slight shift of the maximum and the threshold toward lower velocities. This is consistent with the qualitative arguments put forth in Sec. III G.

Figure 11 shows total fixed-charge stopping powers (target excitation or ionization only) for five charge states ranging from fully stripped to neutral projectiles. It is seen that the stopping power of a neutral projectile is an order of magnitude smaller than that of the stripped ion. Available experimental values of equilibrium stopping powers compiled in Refs. [51,52] have been included for orientation. These data approach calculated stopping powers for stripped ions (O^{8+}) above $E \simeq 3$ MeV/u. This is close to the crossover from the Bohr to the Bethe regime for a bare oxygen ion. The conclusion emerges that for oxygen on carbon the Bethe regime is confined to velocities where the projectile is essentially stripped in charge-state equilibrium.

The energy range depicted in Fig. 11 goes down to 0.1 MeV, which corresponds to $v = v_{\mathrm{TF}}$, i.e., the Thomas-Fermi velocity introduced in Sec. I B or an overall value of $\xi \simeq 0.5$. A substantial Barkas correction may thus be expected near the left end of the graph, which raises the theoretical curves. Qualitatively one would expect $\beta \sim 0.5$ to be appropriate near the Thomas-Fermi velocity. It is clear from Fig. 10 that projectile excitation or ionization cannot contribute noticeably here. The role of electron capture would have to be studied separately.

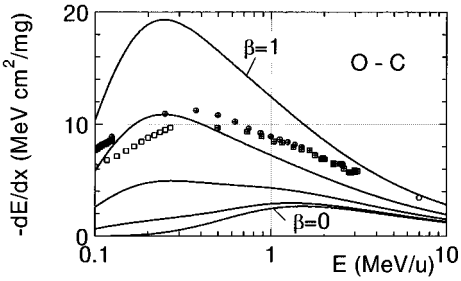

FIG. 11. Comparison of calculated fixed-charge stopping powers with measured equilibrium stopping powers of carbon for oxygen ions. Lines are calculated from modified Bohr theory for charge states $8+$ to 0 in steps of 2 for target excitation and/or ionization only. Experimental points are taken from 14 sets of data compiled in Refs. [51,52].

VI. DISCUSSION

A. Bohr versus Bethe theory

It was shown in Fig. 1 that stopping powers predicted from Bohr's theory for a moving point charge may differ substantially from the corresponding predictions from the Bethe theory. Differences of similar magnitude are found for screened projectiles, but the scaling properties with atomic number and charge state are by no means identical. The two models reflect different velocity regimes for a given ion. Application of either model outside its range of validity may lead to substantial errors.

B. Shell corrections and the Barkas term

Shell corrections originate in the orbital motion of target electrons and become important when the projectile velocity is comparable to or smaller than the orbital speeds v_e in the target shells. The leading term goes as $-\overline{v_e^2}/v^2$ in the Bethe theory [2,53,54] and as

$$-1.5\overline{v_e^2}/v^2 \simeq -\frac{2.9}{(Z_1 Z_2 \xi)^{2/3}}\frac{\overline{v_e^2}}{v_0^2} \tag{57}$$

in the Bohr theory [19]. For $\xi > 1$ and $\overline{v_e^2} \simeq (Z_2^{2/3} v_0)^2$ this implies an upper limit of $\simeq 3(Z_2/Z_1)^{2/3}$. Thus shell corrections are most pronounced for $Z_1 \ll Z_2$, in agreement with experience from light-ion stopping [2].

Barkas corrections, like shell corrections, become significant at low projectile speed. They originate in target polarization by the field of the projectile and scale approximately like $\xi^{-1} = (Z_1 e^2 \omega / m v^3) L'$ [55] in the Bethe regime, with $L' \simeq L_{\mathrm{Bethe}}$ [8]. Unlike the Bloch correction, the Barkas term is sensitive to distant collisions. It is therefore not justified to take over estimates derived for unscreened Coulomb interaction in the analysis. Early estimates of the Barkas effect [55] were performed on the basis of Bohr theory and are therefore applicable to heavy ions, except that they increase rapidly with increasing Z_1 if screening is left out of consideration.

Explicit evaluations of the Barkas effect for a point charge interacting with a quantal harmonic oscillator [56] show a variation with impact parameter very similar to the one predicted from the Bethe theory for the same system [57]. This finding is relevant to heavy-ion stopping since, in the long-distance limit, classical and quantum theory yield equivalent results [58]. One may expect, therefore, a comparable influence of projectile screening on target polarization to what is found for the leading (Bohr) contribution to the stopping cross section.

For stopping powers in the range of $\xi < 1$ the above estimate indicates that Barkas corrections may become substantial. This is relevant to Fig. 11. Another look at the Barkas correction, aiming at moderate or large Z_1 and including screening, may be a prerequisite for reliable theoretical predictions of stopping powers in the velocity range equivalent to $\xi \lesssim 1$.

C. Brandt-Kitagawa theory

A theoretical description of the stopping of a screened ion was developed 15 years ago [22] where the target was modeled as a free electron gas (cf. the Appendix). The range of validity of this theory is limited to the Bethe limit $v \gg 2 Z_1 v_0$.

An electron-gas description is relevant since it is the most weakly bound electrons that have the highest value of s or s' and therefore are most drastically affected by projectile screening. In general, the most weakly bound electrons do not necessarily provide the leading contribution to the stopping power, but Fig. 9 shows that they do so at low projectile speed. Indeed, the applications discussed in Ref. [22] refer mostly to low velocities.

The theory presented in Ref. [22] had a significant impact

and led to further studies and applications along similar lines [5,59,60]. It appears appropriate to mention common features with the present work as well as differences beyond those mentioned already.

The major common feature is the focus on the connection between charge state and stopping power, leaving the determination and incorporation of equilibrium charge-state distributions as a separate problem. The analytic simplicity of exponential screening functions is a very useful feature that emerged from Ref. [22]. The theoretical treatment was based on what has been labeled coherent scattering in the present work.

An effort was made in Ref. [22] to construct a consistent version of the Thomas-Fermi model for exponentially screened ions. That model is possibily more sophisticated than the approach adopted here. It was not utilized here because the description emerging from Ref. [22] differs substantially from standard Thomas-Fermi theory in the limiting case of a neutral atom and because the present description readily allows incorporation of more accurate specific ionic charge distributions.

Apart from this the main difference lies in the scope. The present work focuses on swift heavy ions where several target shells contribute to stopping and where shell corrections are small. Comparatively little attention was given in Ref. [22] to the high-speed behavior. It was mentioned that asymptotically the stopping fraction should approach the form $\mathcal{F}\sim 1+\beta^2/2$ in the present notation. This result follows from Eq. (54) if the second and third terms, which do not depend on the velocity parameter ξ', can be neglected. Note, however, that the logarithmic approach to asymptotic behavior may be quite slow, dependent on the value of s'.

D. q_1^2 scaling and effective charge

In all early and much recent work it is more or less tacitly assumed that the stopping power for an ion is proportional to the square of its charge. Deviations from this relationship were sought in conjunction with higher-order Z_1 effects, i.e., deviations, of the stopping power for a *point charge* from a strict Z_1^2 dependence [15,29,37,49,61,62]. Stopping due to charge exchange causes similar deviations, but can be separated experimentally by measurements at different charge states [41]. However, since the projectile charge ''seen'' by a target electron is impact-parameter dependent, deviations from q_1^2-dependent stopping must be seen even if the stopping cross section for a point charge were strictly proportional to Z_1^2. An initial attempt to quantify this feature dates back to Brandt and Kitagawa [22,63]. That work showed clearly that there is no universally valid relation between the ion charge and the stopping fraction or one of its analogs.

Figure 7 provides clear evidence that the stopping fraction depends equally well on the target as on the ion. There is a wide range of the pertinent parameter set s, β, and ξ where $\mathcal{F}$ is independent of ξ. Deviations from this simple behavior have been found when coherent scattering is assumed and must be expected when Barkas and shell corrections become significant. All these effects enter the low-speed behavior at various stages. However, even in the absence of those complications the need to compute stopping fractions separately for the main target shells makes numerical estimates unnecessarily clumsy compared to straight evaluation of stopping cross sections without going over reference values for a bare ion or a proton. Finally, the physics of the stopping process for a bare ion may differ substantially from that of a screened ion, especially for high Z_1 and low q_1, possibly more than that for proton stopping at the same speed. Hence, although the stopping fraction defined by Eq. (8) is more appropriate than the effective charge defined by Eq. (7) to illustrate the significance of projectile screening on stopping powers and related quantities, neither appears to be a necessary tool in the computation of stopping powers.

ACKNOWLEDGMENTS

Discussions with Henning H. Mikkelsen are gratefully acknowledged. The author thanks H. Paul for having given access to his database on heavy-ion stopping powers. Comments on the manuscript by H. Geissel and J. Lindhard are appreciated. This work has been supported by the Danish Natural Science Research Council (SNF).

APPENDIX: ELECTRON GAS

For completeness it is shown that Eq. (54) also follows from standard stopping theory for a homogeneous electron gas. This case was considered in Refs. [22,25]. Here the established expression for the stopping power [39] has to be appended by a factor $G(Q)$, [Eq. (53)] so that

$$-\frac{dE}{dx}=i\frac{Z_1^2e^2}{\pi v^2}\int_0^\infty\frac{dq}{q}\int_{-qv}^{qv}d\omega\frac{\omega}{\epsilon(q,\omega)}G(Q). \quad \text{(A1)}$$

On the basis of Lindhard's dielectric function for an electron gas at rest [39],

$$\epsilon(q,\omega)=1+\frac{(\hbar\omega_P)^2}{Q^2-(\hbar\omega+i\gamma)^2}, \quad \text{(A2)}$$

with the plasma frequency $\omega_P=\sqrt{4\pi ne^2/m}$, electron density n, and an infinitesimal damping constant γ, the integrations can be performed in closed form, leading to

$$-\frac{dE}{dx}=\frac{2\pi Z_1^2e^4n}{mv^2}\left[\beta^2\ln\frac{Q_+}{Q_-}+(1-\beta^2)\ln\frac{Q_++Q_1}{Q_-+Q_1}-(1-\beta)^2\frac{Q_1(Q_+-Q_-)}{(Q_++Q_1)(Q_-+Q_1)}\right], \quad \text{(A3)}$$

with

$$Q_\pm=mv^2\pm\sqrt{(mv^2)^2-(\hbar\omega_P)^2}. \quad \text{(A4)}$$

This is equivalent to the central result of Ref. [22]. A practical difference originates in the dielectric functions used.

In the limit of $mv^2\gg\hbar\omega_P$ the stopping number per electron reduces to

$$L=\beta^2\ln\frac{2mv^2}{\hbar\omega_P}+(1-\beta^2)\ln\frac{2mva}{\hbar}-\frac{1}{2}(1-\beta)^2, \quad \text{(A5)}$$

which is completely equivalent to Eq. (54).

[1] N. Bohr, Mat. Fys. Medd. K. Dan. Vidensk. Selsk. **18**, No. 8, 1 (1948).
[2] U. Fano, Annu. Rev. Nucl. Sci. **13**, 1 (1963).
[3] L. C. Northcliffe, Annu. Rev. Nucl. Sci. **13**, 67 (1963).
[4] P. Sigmund, in *Radiation Damage Processes in Materials*, Vol. 8 of *NATO Advanced Study Institutes, Series E: Applied Sciences*, edited by C. H. S. Dupuy (Noordhoff, Leyden, 1975), pp. 3–117.
[5] J. F. Ziegler, J. P. Biersack, and U. Littmark, *The Stopping and Range of Ions in Solids* (Pergamon, New York, 1985), Vol. 1.
[6] J. Lindhard, V. Nielsen, and M. Scharff, Mat. Fys. Medd. K. Dan. Vidensk. Selsk. **36**, No. 10, 1 (1968).
[7] H. Bethe, Ann. Phys. (Leipzig) **5**, 324 (1930).
[8] J. Lindhard, Nucl. Instrum. Methods **132**, 1 (1976).
[9] F. Bloch, Ann. Phys. (Leipzig) **16**, 285 (1933).
[10] *Handbook of Mathematical Functions*, edited by M. Abramowitz and I. A. Stegun (Dover, New York, 1964).
[11] J. Lindhard and A. H. Sørensen, Phys. Rev. A **53**, 2443 (1996).
[12] N. Bohr, Philos. Mag. **25**, 10 (1913).
[13] L. C. Northcliffe and R. F. Schilling, Nucl. Data, Sect. A **7**, 233 (1970).
[14] F. Hubert, A. Fleury, R. Bimbot, and D. Gardes, Ann. Phys. (Paris) **5**, 1 (1980).
[15] J. F. Ziegler, *Handbook of Stopping Cross Sections for Energetic Ions in All Elements* (Pergamon, New York, 1980), Vol. 5.
[16] F. Hubert, R. Bimbot, and H. Gauvin, At. Data Nucl. Data Tables **46**, 1 (1990).
[17] J. M. Anthony and W. A. Lanford, Phys. Rev. A **25**, 1868 (1982).
[18] J. Lindhard and M. Scharff, Mat. Fys. Medd. K. Dan. Vidensk. Selsk. **27**, No. 15, 1 (1953).
[19] P. Sigmund, Phys. Rev. A **54**, 3113 (1996).
[20] N. Bohr, Phys. Rev. **58**, 654 (1940).
[21] J. Knipp and E. Teller, Phys. Rev. **59**, 659 (1941).
[22] W. Brandt and M. Kitagawa, Phys. Rev. B **25**, 5631 (1982).
[23] Y. K. Kim and K. T. Cheng, Phys. Rev. A **22**, 61 (1980).
[24] O. H. Crawford, Phys. Rev. A **39**, 4432 (1989).
[25] A. Arnau and P. M. Echenique, Nucl. Instrum. Methods Phys. Res. B **42**, 165 (1989).
[26] K. B. Winterbon, Nucl. Instrum. Methods **144**, 311 (1977).
[27] P. Sigmund, Nucl. Instrum. Methods Phys. Res. B **69**, 113 (1992).
[28] P. Sigmund, Phys. Rev. A **50**, 3197 (1994).
[29] N. E. B. Cowern *et al.*, Phys. Rev. A **30**, 1682 (1984).
[30] F. Bloch, Z. Phys. **81**, 363 (1933).
[31] R. E. Johnson, *Introduction to Atomic and Molecular Collisions* (Plenum, New York, 1982), Appendix C.
[32] J. S. Briggs and K. Taulbjerg, in *Structure and Collisions of Ions and Atoms*, edited by I. A. Sellin, Current Topics in Physics Vol. 5 (Springer, Berlin, 1978), Chap. 4, pp. 105–153.
[33] N. M. Kabachnik, J. Phys. B **26**, 3803 (1993).
[34] P. Gombas, in *Handbuch der Physik*, edited by S. Flügge (Springer, Berlin, 1956), Vol. 36, pp. 109–231.
[35] E. Fermi, Mem. Accad. Italia **1**, 1 (1930).
[36] E. Fermi and E. Amaldi, Mem. Accad. Italia **6**, 117 (1934).
[37] S. Datz *et al.*, Phys. Rev. Lett. **38**, 1145 (1977).
[38] M. Inokuti, Argonne National Laboratory Report No. ANL-76-88, 1976, p. 177 (unpublished).
[39] J. Lindhard, Mat. Fys. Medd. K. Dan. Vidensk. Selsk. **28**, No. 8, 1 (1954).
[40] N. E. B. Cowern *et al.*, Nucl. Instrum. Methods Phys. Res. B **2**, 112 (1984).
[41] N. E. B. Cowern, P. M. Read, and C. J. Sofield, Nucl. Instrum. Methods Phys. Res. B **12**, 43 (1985).
[42] C. M. Frey *et al.*, Nucl. Instrum. Methods Phys. Res. B **107**, 31 (1996).
[43] J. L. Dehmer, M. Inokuti, and R. P. Saxon, Phys. Rev. A **12**, 102 (1975).
[44] M. Inokuti, J. L. Dehmer, L. T. Baer, and J. D. Hanson, Phys. Rev. A **23**, 95 (1981).
[45] J. Oddershede and J. R. Sabin, At. Data Nucl. Data Tables **31**, 275 (1984).
[46] S. K. Allison, J. Cuevas, and M. Garcia-Munos, Phys. Rev. **127**, 792 (1962).
[47] J. Cuevas, M. Garcia-Munos, P. Torres, and S. K. Allison, Phys. Rev. **135**, A335 (1964).
[48] H. Ogawa *et al.*, Nucl. Instrum. Methods Phys. Res. B **69**, 108 (1992).
[49] J. A. Golovchenko *et al.*, Phys. Rev. B **23**, 957 (1981).
[50] J. U. Andersen *et al.*, Nucl. Instrum. Methods Phys. Res. B **90**, 104 (1994).
[51] M. J. Berger and H. Paul, *Atomic and Molecular Data for Radiotherapy and Radiation Research* (International Atomic Energy Agency, Vienna, 1995), No. IAEA-TECDOC-799, Chap. 7, pp. 415–546.
[52] H. Paul (unpublished).
[53] J. Lindhard and A. Winther, Mat. Fys. Medd. K. Dan. Vidensk. Selsk. **34**, No. 4, 1 (1964).
[54] P. Sigmund, Phys. Rev. A **26**, 2497 (1982).
[55] J. C. Ashley, R. H. Ritchie, and W. Brandt, Phys. Rev. B **5**, 2393 (1992).
[56] H. H. Mikkelsen and P. Sigmund, Phys. Rev. A **40**, 101 (1989).
[57] H. H. Mikkelsen and P. Sigmund, Nucl. Instrum. Methods Phys. Res. B **27**, 266 (1987).
[58] K. W. Hill and E. Merzbacher, Phys. Rev. A **9**, 156 (1974).
[59] R. J. Mathar and M. Posselt, Phys. Rev. B **51**, 107 (1995).
[60] Q. Yang, Phys. Rev. A **49**, 1089 (1994).
[61] B. S. Yarlagadda, J. E. Robinson, and W. Brandt, Phys. Rev. B **17**, 3473 (1978).
[62] H. H. Andersen, in *Semiclassical Descriptions of Atomic and Nuclear Collisions*, edited by J. Bang and J. D. Boor (North-Holland, Amsterdam, 1985), pp. 409–430.
[63] W. Brandt, Nucl. Instrum. Methods **194**, 13 (1982).